Engineering Analysis with Boundary Elements 60 (2015) 144–153

Contents lists available at ScienceDirect

Engineering Analysis with Boundary Elements

journal homepage: www.elsevier.com/locate/enganabound

Calculation of 2D nearly singular integrals over high-order geometry elements using the sinh transformation

Yaoming Zhang [a,b,*], Yanpeng Gong [a], Xiaowei Gao [b]

[a] Institute of Applied Mathematics, Shandong University of Technology, Zibo 255049, Shandong Province, PR China
[b] State Key Laboratory of Structural Analysis for Industrial Equipment, Dalian University of Technology, Dalian 116024, PR China

ARTICLE INFO

Article history:
Received 14 November 2014
Received in revised form
23 December 2014
Accepted 23 December 2014
Available online 3 February 2015

Keywords:
3D BEM
Nearly singular integrals
Sinh transformation
Boundary layer effect
Thin-structural problem

ABSTRACT

The accurate evaluation of nearly singular integrals plays an important role in the implementation of BEM. In general, these include evaluating the solution near the boundary or treating problems with thin domains, which are respectively named the boundary layer effect and the thin-body effect in BEM. Although many methods of evaluating two-dimensional (2D) nearly singular integrals have been developed in recent years with varying degrees of success, questions still remain. In this paper, we present an efficient strategy for numerical evaluation of 2D nearly singular integrals that arise in the solution of 3D BEM using eight-node second-order quadrilateral surface elements. The strategy is an extension of the sinh transformation, which is used to evaluate the 1D or 2D nearly singular integrals on simple geometry elements, such as usual linear or planar elements. Several numerical examples involving boundary layer effect and thin body problems in 3D potential problems are investigated to verify the proposed scheme, yielding very promising results.

1. Instruction

The accurate evaluation of nearly singular integrals is one of the major concerned problems in the boundary element method (BEM) [1–7]. Nearly singular integrals usually exist in two situations, known as, boundary layer effect problems and thin-body problems. The boundary layer effect refers to the phenomenon such that the field variables and their derivatives at the point near the boundary cannot be computed accurately with the ordinary Gaussian quadratures owing to the nearly singular properties of the integral kernels. In engineering, efficient solution of the boundary layer effect has wide applications; in general, these include evaluating the solution near the boundary in potential problems and calculating displacements and stresses near the boundary in elasticity problems, for example, displacement around open crack tips, contact problems, sensitivity problems, etc. Thin-body structures are frequently used for the design of various industrial applications, including solid mechanics, acoustics and electromagnetism. The advantage of these structures relies on their principal character: the thickness, which is a natural optimization strategy based on reducing dead loads and minimizing construction material usage. Studies show that the conventional boundary element method using the standard Gaussian quadrature fails to yield reliable results for these structures. The major reason for this failure is that the kernels' integration presents various orders of near singularities, owing to the mesh on one side of the thin body being too close to the mesh on the opposite side.

In the past decades, tremendous effort was devoted to derive convenient integral forms or sophisticated computational techniques for evaluating nearly singular integrals, among which the variable transformations technique, based on various nonlinear functions, seems to be a more promising approach owing to its successful numerical tests carried out on various examples. The methods developed so far include, but are not limited to, polynomial transformation [8,9], degenerate mapping method [10], coordinate optimal transformation [11], sigmoidal transformation [12,13], sinh transformation [13–19], rational transformation [20], distance transformation [21–24], exponential transformation [25–30] and combinations of the polar coordinates approach with variable transformations [13]. Although great progresses have been achieved for each of the above methods, a number of drawbacks remains and mainly include the fact that some, which benefit from the strategies for calculating the singular integrals, are failed to fully eliminate near singularities, some apply only to the planar elements, some construct a simple but approximate distance function, which usually results from the first-order Taylor expansion approximation of surface geometry element, and thus

* Corresponding author at: Institute of Applied Mathematics, Shandong University of Technology, Zibo 255049, Shandong Province, PR China.
E-mail address: zymfc@163.com (Y. Zhang).

http://dx.doi.org/10.1016/j.enganabound.2014.12.006
0955-7997/

its accuracy is nonuniformly distributed on the integration element, and others are tailored to a certain kind of integrals and therefore lack wide applicability. In this work, we focus on the sinh transformation, proposed by Johnston and Elliott [14].

For the sinh transformation, based on the sinh function, its advantages, such as accuracy, stability, wide applicability and ease implementation have been demonstrated on a large number of numerical test examples [13–19]. However, in the 3D BEM, most of the existing methods share the feature of evaluating the nearly singular integrals that are only defined on planar geometry element. To date, very few studies on the calculation of nearly singular integrals over curved surface have been reported in the BEM community [30]. Johnston and Elliott [15–17] has proposed an efficient strategy to numerically compute the nearly singular integrals over the 9-point Lagrangian curved surface element in 3D BEM using the sinh transformation, and Miao Yu and his co-workers [18,19] also have done further researches on this topic. Nevertheless, it is worth noting that, in their studies, only simple test integrals on a single element, based on a specified 'projection point', have been examined, and no application in practical BEM problems has been found as yet, although these strategies seem to have such potential [30].

Inspired by the pioneering work mentioned above, we here extend the sinh transformation to evaluate 2D nearly singular integrals over eight-node second-order quadrilateral surface elements arising in 3D BEM. The main novel features of the proposed method lie in (1) developing a 'proper' distance formula, as in Ref. [30]. Such distance formula is easy to combine with the sinh transformation. Next, it is able to accurately approximate the actual distance, r, from the source point to a generic point of the element, which usually derives from the first-order Taylor expansion approximation of curved surface element in other approaches. So promising results for numerical evaluation of 2D nearly singular integrals can be expected; (2) ingenious combination of the aforementioned distance formula with the sinh transformation. The sinh transformation can smooth out the rapid variation of the developed distance formula on integration interval.

The outline of the rest of this paper is as follows. The general form of nearly singular integrals is described in Section 2. Then, in Section 3, the distance function, based on the eight-node second-order quadrilateral surface elements, is constructed. Section 4 considers the regularization of nearly singular integrals over high-order geometrical elements using the sinh transformation. In Section 5, the accuracy and stability of the proposed scheme are tested on three 3D potential examples with known benchmark solutions. Finally, the conclusions are provided in Section 6.

2. General descriptions

For 3D potential problems in the domain Ω enclosed by boundary Γ, without regard to the body sources, the regularized boundary integral equation can be expressed in terms of the flux $q=\partial u/\partial n$ and potential u on the boundary as follows:

$$\int_\Gamma q(\boldsymbol{x})u^*(\boldsymbol{x},\boldsymbol{y})d\Gamma_x=\int_\Gamma [u(\boldsymbol{x})-u(\boldsymbol{y})]q^*(\boldsymbol{x},\boldsymbol{y})d\Gamma_x. \tag{1}$$

For the internal point $\boldsymbol{y}$, the integral equations are written as

$$u(\boldsymbol{y})=\int_\Gamma q(\boldsymbol{x})u^*(\boldsymbol{x},\boldsymbol{y})d\Gamma_x-\int_\Gamma u(\boldsymbol{x})q^*(\boldsymbol{x},\boldsymbol{y})d\Gamma_x, y\in\Omega \tag{2}$$

$$\nabla u(\boldsymbol{y})=\int_\Gamma q(\boldsymbol{x})\nabla u^*(\boldsymbol{x},\boldsymbol{y})d\Gamma_x-\int_\Gamma u(\boldsymbol{x})\nabla q^*(\boldsymbol{x},\boldsymbol{y})d\Gamma_x, \boldsymbol{y}\in\Omega. \tag{3}$$

In Eqs. (1)–(3), $\boldsymbol{y}$ and $\boldsymbol{x}$ are the source and the field points, respectively; $u^*(\boldsymbol{x},\boldsymbol{y})$ denotes the Kelvin fundamental solution for 3D potential problems expressed as

$$u^*(\boldsymbol{x},\boldsymbol{y})=\frac{1}{4\pi r} \tag{4}$$

and $q^*(\boldsymbol{x},\boldsymbol{y})$ is the derived fundamental solution

$$q^*(\boldsymbol{x},\boldsymbol{y})=\frac{\partial u^*(\boldsymbol{x},\boldsymbol{y})}{\partial \boldsymbol{n}} \tag{5}$$

where $\boldsymbol{n}$ is the unit outward normal direction to the boundary Γ, with components $n_i,\ i=1,\ 2,\ 3$.

For the discretized form of the Eqs. (1)–(3), when the source point $\boldsymbol{y}$ is far enough from the integration elements, a straightforward application of Gaussian quadrature procedure suffices to evaluate such integrals. However, when the source point $\boldsymbol{y}$ is very close to but not on the integration elements Γ_e, nearly singular integrals arise with different levels, and the numerical integrations by the standard Gaussian quadrature fail. These nearly singular integrals can be expressed as

$$I=\int_{\Gamma_e}\frac{f(\boldsymbol{x},\boldsymbol{y})}{r^\alpha}d\Gamma_x \tag{6}$$

where $r=\|\boldsymbol{x}-\boldsymbol{y}\|_2$, $\alpha>0$ is a real constant, and $f(\boldsymbol{x},\boldsymbol{y})$ denotes a well-behaved function which consists of shape function, Jacobian and coefficients from the derivation of the kernels.

3. Nearly singular integrals on high-order geometry elements

To numerically evaluate boundary integrals for Eqs. (1)–(3), the boundary Γ is divided into a number of surface segments, which are called boundary elements. Two approximations are made over each of these elements. One is about the geometry of the boundary, while the other has to interpolate the spatial variation of the field variables or the boundary unknowns over the element. The plane shape geometry element is not an ideal one as it cannot approximate the curved surface boundaries with sufficient accuracy. For this reason, it is recommended to use higher order elements, which approximate geometry and boundary quantities by using higher order interpolation polynomials-usually of the second order.

In this paper, the geometry segment is modeled by a continuous paraboloidal element, which has eight knots, namely, the boundary geometry is approximated by the piecewise continuous eight-node second-order quadrilateral surface elements, while the distribution of the boundary quantities over each of these segments is approximated using discontinuous elements, eight nodes of which are located away from the edges of the element.

Assume $x^j=(x_1^j,\ x_2^j,\ x_3^j),\quad j=1,\ \ldots,\ 8$ are the eight knots of the element of the segment Γ_j, then Cartesian coordinates of the points on the element Γ_j can be interpolated as follows:

$$x_k(\xi_1,\xi_2)=\sum_{j=1}^{8}N_j(\xi_1,\xi_2)x_k^j,\quad k=1,\ 2,\ 3 \tag{7}$$

where

$$N_1(\xi_1,\xi_2)=\tfrac{1}{4}(1-\xi_1)(1-\xi_2)(-\xi_1-\xi_2-1),\quad N_2(\xi_1,\xi_2)=\tfrac{1}{4}(1+\xi_1)(1-\xi_2)(\xi_1-\xi_2-1)$$

$$N_3(\xi_1,\xi_2)=\tfrac{1}{4}(1+\xi_1)(1+\xi_2)(\xi_1+\xi_2-1),\quad N_4(\xi_1,\xi_2)=\tfrac{1}{4}(1-\xi_1)(1+\xi_2)(-\xi_1+\xi_2-1)$$

$$N_5(\xi_1,\xi_2)=\tfrac{1}{2}(1-\xi_1^2)(1-\xi_2),\quad N_6(\xi_1,\xi_2)=\tfrac{1}{2}(1+\xi_1)(1-\xi_2^2)$$

$$N_7(\xi_1,\xi_2)=\tfrac{1}{2}(1+\xi_2)(1-\xi_1^2),\quad N_8(\xi_1,\xi_2)=\tfrac{1}{2}(1-\xi_1)(1-\xi_2^2),-1\le\xi_1\le 1,\quad -1\le\xi_2\le 1$$

here, $\xi_1,\ \xi_2$ are the dimensionless coordinates. And the boundary function $\phi(\boldsymbol{x})$ is approximated using second-order discontinuous interpolating function, i.e.

$$\phi(\boldsymbol{x})\approx\sum_{k=1}^{8}N_k(\xi_1/\beta,\xi_2/\beta)\phi^k \tag{8}$$

where β is always taken as 0.5 in this paper (as the author previous papers). ϕ^k denotes the value of boundary function $\phi(\boldsymbol{x})$ on the kth interpolation node.

3.1. Determination of the projection point

The minimum distance d from the source point $\boldsymbol{y}$ to the integration element Γ_e is defined as the length $|\boldsymbol{y}-\boldsymbol{x}^p|$, where $\boldsymbol{x}^p$ is the projection point of $\boldsymbol{y}$ onto integration element Γ_e. Letting $(\eta_1,\ \eta_2)$ be the local coordinates of the projection point $\boldsymbol{x}^p$, i.e. $\boldsymbol{x}^p=(x_1(\eta_1,\eta_2),\ x_2(\eta_1,\eta_2),\ x_3(\eta_1,\eta_2))$, then $\eta_1,\ \eta_2$ are the real roots of the following equation:

$$\begin{cases}[x_i(\eta_1,\eta_2)-y_i]\dfrac{\partial x_i}{\partial \xi_1}=0\\ [x_i(\eta_1,\eta_2)-y_i]\dfrac{\partial x_i}{\partial \xi_2}=0\end{cases},\quad i=1,2,3 \tag{9}$$

in which the summation convention is used, and $(\partial x_i/\partial\xi_k)=(\partial x_i/\partial\xi_k)|_{\substack{\xi_1=\eta_1\\ \xi_2=\eta_2}},\quad k=1,\ 2$. These assumptions will be applied also in what follows unless specified others.

If the source point $\boldsymbol{y}$ is sufficiently close to the boundary Γ_e, then $\boldsymbol{x}^p$ is inside the integration element, and Eq. (9) has a pair of the unique real roots $(\eta_1,\ \eta_2)\in[-1,1][-1,1]$. The real roots $\eta_1,\ \eta_2$ can be evaluated numerically by using Newton's method. Setting

$$f_1(\eta_1,\eta_2)=[x_i(\eta_1,\eta_2)-y_i]\frac{\partial x_i}{\partial\xi_1},\quad f_2(\eta_1,\eta_2)=[x_i(\eta_1,\eta_2)-y_i]\frac{\partial x_i}{\partial\xi_2}$$

The formula of Newton's method can be expressed as

$$F'(\boldsymbol{\eta}^{(k)})\Delta\boldsymbol{\eta}^{(k)}=-F(\boldsymbol{\eta}^{(k)}) \tag{10}$$

where

$$\Delta\boldsymbol{\eta}^{(k)}=\boldsymbol{\eta}^{(k+1)}-\boldsymbol{\eta}^{(k)},\quad \boldsymbol{\eta}^{(k)}=(\eta_1{}^{(k)},\eta_2{}^{(k)})^{\mathrm{T}},$$
$$\boldsymbol{\eta}^{(k+1)}=(\eta_1{}^{(k+1)},\eta_2{}^{(k+1)})^{\mathrm{T}},$$
$$F(\boldsymbol{\eta}^{(k)})=\begin{bmatrix}f_1(\eta_1{}^{(k)},\eta_2{}^{(k)})\\ f_2(\eta_1{}^{(k)},\eta_2{}^{(k)})\end{bmatrix},\quad F'(\boldsymbol{\eta}^{(k)})=\begin{bmatrix}\frac{\partial f_1}{\partial\eta_1} & \frac{\partial f_1}{\partial\eta_2}\\ \frac{\partial f_2}{\partial\eta_1} & \frac{\partial f_2}{\partial\eta_2}\end{bmatrix}_{\boldsymbol{\eta}=\boldsymbol{\eta}^{(k)}}$$

here

$$\frac{\partial f_j}{\partial\eta_m}=\sum_i^3\left(\frac{\partial x_i}{\partial\xi_m}\frac{\partial x_i}{\partial\xi_j}+[x_i(\eta_1,\eta_2)-y_i]\frac{\partial^2 x_i}{\partial\xi_j\,\partial\xi_m}\right),\quad j,\ m=1,\ 2.$$

3.2. Construction of distance functions

$x_k(\xi_1,\xi_2)$ can be expressed as follows:

$$x_k(\xi_1,\xi_2)=x_k(\eta_1,\eta_2)+(\xi_\alpha-\eta_\alpha)\frac{\partial x_k}{\partial\xi_\alpha}+\tfrac{1}{2}(\xi_\alpha-\eta_\alpha)(\xi_\beta-\eta_\beta)\frac{\partial^2 x_k}{\partial\xi_\alpha\,\partial\xi_\beta},$$
$$(\alpha,\ \beta=1,\ 2) \tag{11}$$

thus, we have

$$\begin{aligned}r^2(\xi_1,\xi_2)=d^2&+(\xi_\alpha-\eta_\alpha)\tilde g_\alpha+(\xi_\alpha-\eta_\alpha)\left(\xi_\beta-\eta_\beta\right)\tilde g_{\alpha\beta}\\&+(\xi_\alpha-\eta_\alpha)\left(\xi_\beta-\eta_\beta\right)\left(\xi_\gamma-\eta_\gamma\right)\tilde g_{\alpha\beta\gamma}\\&+(\xi_\alpha-\eta_\alpha)\left(\xi_\beta-\eta_\beta\right)\left(\xi_\gamma-\eta_\gamma\right)\left(\xi_\mu-\eta_\mu\right)\tilde g_{\alpha\beta\gamma\mu}\end{aligned} \tag{12}$$

where the summation rule is applied with respect to the Latin indices (taken from the range 1, 2, 3) and Greek indices (taken from the range 1, 2)

$$d^2=(y_k-x_k^p)(y_k-x_k^p),\tilde g_\alpha=2(y_k-x_k^p)x_{k,\alpha},$$
$$x_{k,\alpha}=\left.\frac{\partial x_k}{\partial\xi_\alpha}\right|_{\xi_1=\eta_1}$$
$$\xi_2=\eta_2,\tilde g_{\alpha\beta}=\tilde g_{\beta\alpha}=(y_k-x_k^p)x_{k,\alpha\beta}+x_{k,\alpha}x_{k,\beta}$$
$$\tilde g_{\alpha\beta\gamma}=\tilde g_{\beta\alpha\gamma}=x_{k,\alpha\beta}x_{k,\gamma},\tilde g_{\alpha\beta\gamma\mu}=\tilde g_{\beta\alpha\gamma\mu}=\tfrac{1}{4}x_{k,\alpha\beta}x_{k,\gamma\mu}.$$

Recall that $\tilde g_\alpha\equiv 0$, since $(y_k-x_k^p)$ is orthogonal to the element and $x_{k,\alpha}$ is tangential to the element at the projection point $\boldsymbol{x}^p$. Thus, Eq. (12) can be rewritten as

$$\begin{aligned}r^2(\xi_1,\xi_2)&=d^2+(\xi_\alpha-\eta_\alpha)\left(\xi_\beta-\eta_\beta\right)\hat g_{\alpha\beta}\\&=d^2+(\xi_1-\eta_1)^2g_{11}+(\xi_2-\eta_2)^2g_{22}+(\xi_1-\eta_1)(\xi_2-\eta_2)g_{12}\end{aligned} \tag{13}$$

where

$$\hat g_{\alpha\beta}=\tilde g_{\alpha\beta}+(\xi_\gamma-\eta_\gamma)\tilde g_{\alpha\beta\gamma}+(\xi_\gamma-\eta_\gamma)(\xi_\mu-\eta_\mu)\tilde g_{\alpha\beta\gamma\mu},$$
$$g_{11}=\hat g_{11},\quad g_{22}=\hat g_{22},\quad g_{12}=\hat g_{12}+\hat g_{21}=2\hat g_{12}.$$

3.3. Form of nearly singular integrals on the second-order elements

By some simple deductions and based on the expression form (13) of the distance function r^2, the nearly singular integrals in Eq. (6) would be reduced to the following form:

$$I=\int_0^B\int_0^A\frac{f(u,v)}{[d^2+u^2g_{11}(u,v)+uvg_{12}(u,v)+v^2g_{22}(u,v)]^\alpha}du\,dv \tag{14}$$

where A and B are the two constants which have possibly different values in different integrals; $f(\cdot)$ is a regular function that consists of shape functions, Jacobian and terms which arise from taking the derivative of the integral kernels.

4. The sinh transformation

The sinh transformation has been proved to be feasible in dealing with the nearly singular linear integrals over planar elements [13–17]. In this paper, the sinh transformation is extended to treat the nearly singular surface integrals over paraboloidal surface elements in 3D BEM.

For the integrals in Eq. (14), the proposed transformation can be expressed as follows:

$$u=d\sinh(m_1+m_2s),\quad v=d\sinh(n_1+n_2t),\quad -1\le s\le 1,\ -1\le t\le 1 \tag{15}$$

where $m_1=m_2=(1/2)\mathrm{arcsinh}(A/d)$, $n_1=n_2=(1/2)\mathrm{arcsinh}(B/d)$.

The Jacobian of the transformation (15) is then given by

$$|J|=d^2m_2n_2\cosh(m_1+m_2s)\cosh(n_1+n_2t)$$

hence, we obtain the following equation:

$$I=\frac{1}{d^{2\alpha-2}}\int_{-1}^1\int_{-1}^1\frac{f(s,t)d^2m_2n_2\cosh(m_1+m_2s)\cosh(n_1+n_2t)}{F^\alpha(s,t)}ds\,dt \tag{16}$$

where

$$\begin{aligned}F(s,t)=1&+(\sinh(m_1+m_2s))^2g_{11}(u,v)+(\sinh(n_1+n_2t))^2g_{22}(u,v)\\&+\sinh(m_1+m_2s)\sinh(n_1+n_2t)g_{12}(u,v)\end{aligned}$$

with u an v being given by Eq. (15).

5. Numerical examples

In order to demonstrate the effectiveness and robustness of the proposed scheme, several numerical examples involving boundary layer effect and thin body problems are investigated below. The eight-node second-order quadrilateral surface elements are employed to depict the geometry boundary, and the same type of discontinuous interpolation functions to approximate the boundary functions.

Sufficient numerical results are obtained even when the distance between the evaluation point and the boundary element is very small. The results obtained by using the present method as well as by the conventional algorithm (without any transformation) and the exact solutions are all presented for convenience of comparison.

The average relative error (ARE) of the multiple computational results for many computing points is defined by the following equation:

$$\mathrm{ARE}=\sqrt{\sum_{k=1}^{M}\left(I_{num}^{k}-I_{exact}^{k}\right)^{2}\Big/\sum_{k=1}^{M}\left|I_{exact}^{k}\right|^{2}}$$

where I_{num}^{k} and I_{exact}^{k} denote the numerical and exact value at the kth point, respectively, and M is the number of the interior evaluation points. In particular, when $M=1$, the symbol RE is used instead of ARE to more accurately denote the relative error at one single evaluation point.

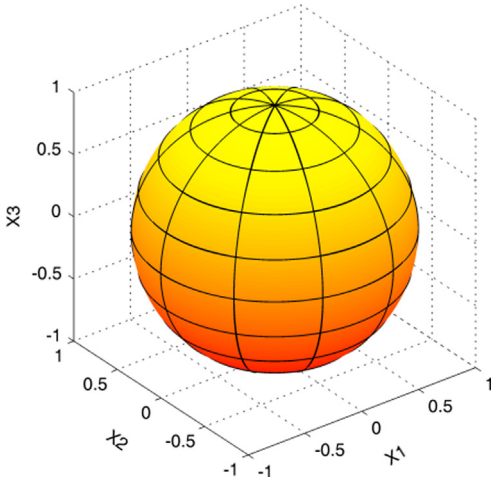

Fig. 1. Discretization of a unit sphere with 100 second-order surface elements.

In what follows, d denotes the distance between the evaluation point and the integration boundary element.

Example 1 As shown in Fig. 1, this example concerns a three dimensional spherical structure with radius 1.0. The prescribed temperature on the boundary is

$$u=x^2-y^2+2x+z$$

The spherical surface is divided into 100 (10×10) surface elements of the second-order, and the same type of discontinuous interpolation shape functions is adopted to approximate the boundary functions. The numerical solutions for the potentials u and their derivatives $\partial u/\partial x_1$ (in the x_1 direction) at internal points whose projection points are on the 41th element are listed in Tables 1 and 2, respectively, hence we can see that when the evaluation points are not too close to the boundary, both the methods with and without transformation of the integration variables are effective and can give acceptable results. As the evaluation point approaches the boundary element of integration, i.e., when the distance of the internal point from the integration element is equal to or less than 0.001, the results of the conventional method become less satisfactory. On the other hand, the results of the proposed method are still steady and satisfactory even when the distance of the evaluation point to the integration element reaches $1E-12$. This can be seen from the relative errors with respect to the exact solutions which are also shown in Tables 1 and 2 and demonstrate the efficiency and the usefulness of the developed algorithm.

Table 1
Potentials u at internal points increasingly close to the boundary.

Distance d	Exact	No transformation	Present	
			Numerical	Error
0.1	0.1248193E+01	0.1248727E+01	0.1248592E+01	0.3200846E−03
0.01	0.2607711E+01	0.2607939E+01	0.2606614E+01	0.4205531E−03
0.001	0.2957702E+01	0.2950826E+01	0.2956300E+01	0.4741605E−03
0.0001	0.2993592E+01	0.2960695E+01	0.2992212E+01	0.4609367E−03
0.00001	0.2997190E+01	0.2959677E+01	0.2995813E+01	0.4593487E−03
0.000001	0.2997550E+01	0.2959552E+01	0.2996174E+01	0.4591865E−03
0.0000001	0.2997586E+01	0.2959539E+01	0.2996210E+01	0.4591617E−03
0.00000001	0.2997590E+01	0.2959538E+01	0.2996213E+01	0.4591383E−03
0.000000001	0.2997590E+01	0.2959538E+01	0.2996214E+01	0.4591248E−03
0.0000000001	0.2997590E+01	0.2959538E+01	0.2996214E+01	0.4591756E−03
0.00000000001	0.2997590E+01	0.2959538E+01	0.2996213E+01	0.4593694E−03
0.000000000001	0.2997590E+01	0.2959538E+01	0.2996212E+01	0.4597946E−03

Table 2
Potential derivatives $\partial u/\partial x_1$ at internal points increasingly close to the boundary.

Distance d	Exact	No transformation	Present	
			Numerical	Error
0.01	0.3978795E+01	0.2634926E+01	0.3980482E+01	0.4239586E−03
0.001	0.3996795E+01	−0.8982565E+00	0.3980482E+01	0.4239586E−03
0.0001	0.3998595E+01	−0.1363919E+01	0.4000152E+01	0.8400486E−03
0.00001	0.3998775E+01	−0.1410545E+01	0.4002129E+01	0.8838143E−03
0.000001	0.3998793E+01	−0.1415207E+01	0.4002327E+01	0.8884301E−03
0.0000001	0.3998795E+01	−0.1415673E+01	0.4002356E+01	0.8911755E−03
0.00000001	0.3998795E+01	−0.1415720E+01	0.4002372E+01	0.8946804E−03
0.000000001	0.3998795E+01	−0.1415725E+01	0.4002379E+01	0.8962263E−03
0.0000000001	0.3998795E+01	−0.1415725E+01	0.4002297E+01	0.8757364E−03
0.00000000001	0.3998795E+01	−0.1415725E+01	0.4002254E+01	0.8650381E−03
0.000000000001	0.3998795E+01	−0.1415725E+01	0.4001767E+01	0.7432272E−03

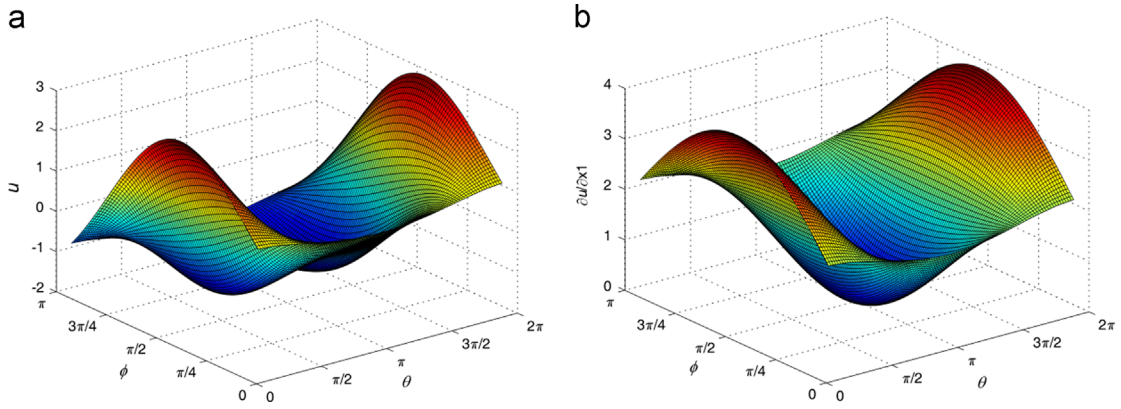

Fig. 2. Profiles of analytical solutions for the potentials (a) and their derivatives (b).

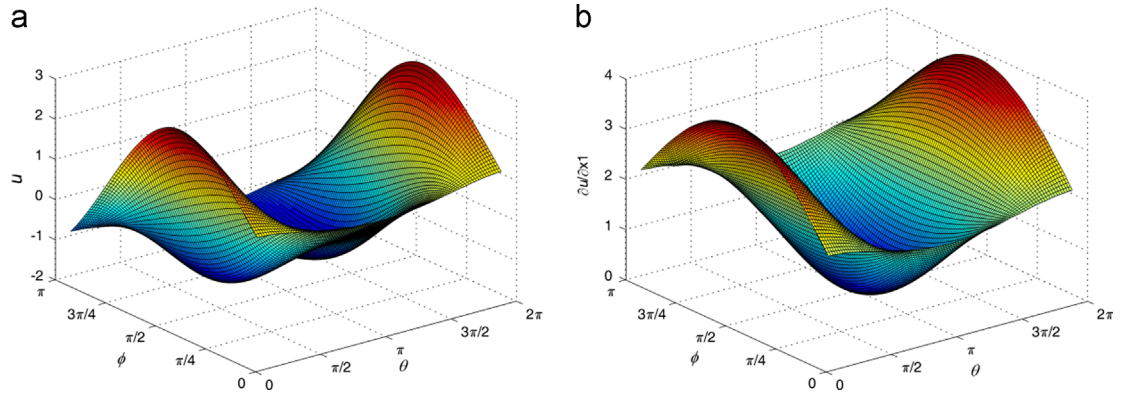

Fig. 3. Surfaces of numerical solutions for the potentials (a) and their derivatives (b).

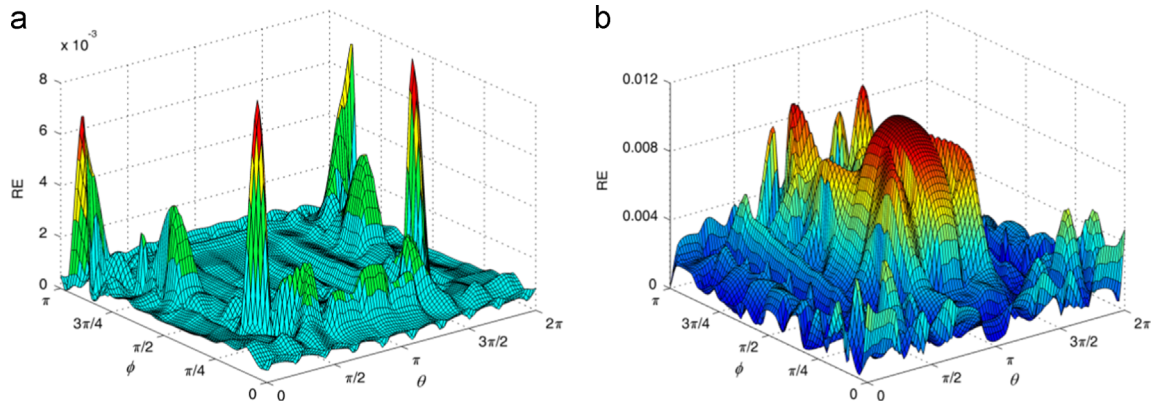

Fig. 4. Surfaces of REs for the potentials (a) and their derivatives (b).

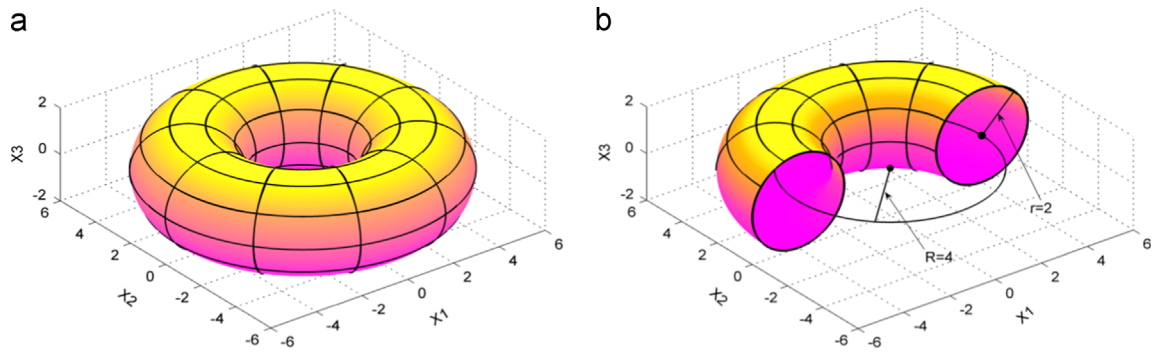

Fig. 5. Discretization of the torus with 98 second-order surface elements.

Table 3
Potentials u at internal points along x_1 axis.

Interior points	Exact	No transformation	Present	
			Numerical	Error
(2.005, 0, 0)	0.1203501E+02	0.1204975E+02	0.1203022E+02	0.3983161E−03
(2.006, 0, 0)	0.1204202E+02	0.1205591E+02	0.1203723E+02	0.3972977E−03
(2.008, 0, 0)	0.1205603E+02	0.1206833E+02	0.1205127E+02	0.3952628E−03
(2.01, 0, 0)	0.1207005E+02	0.1208086E+02	0.1206530E+02	0.3932303E−03
(2.08, 0, 0)	0.1256320E+02	0.1256157E+02	0.1255912E+02	0.3243663E−03
(2.8, 0, 0)	0.1792000E+02	0.1791956E+02	0.1791956E+02	0.2467728E−04
(3.5, 0, 0)	0.2362500E+02	0.2362467E+02	0.2362448E+02	0.2186995E−04
(4.0, 0, 0)	0.2800000E+02	0.2799950E+02	0.2799941E+02	0.2119833E−04
(4.4, 0, 0)	0.3168000E+02	0.3167967E+02	0.3166672E+02	0.4191201E−03
(5.9, 0, 0)	0.4690500E+02	0.4691849E+02	0.4686514E+02	0.8498257E−03
(5.99, 0, 0)	0.4789005E+02	0.4744910E+02	0.4785551E+02	0.7213234E−03
(5.995, 0, 0)	0.4794501E+02	0.4742090E+02	0.4791083E+02	0.7129915E−03

Table 4
Potential derivatives $\partial u/\partial x_1$ at internal points along x_1 axis.

Interior points	Exact	No transformation	Present	
			Numerical	Error
(2.005, 0, 0)	0.7005000E+01	0.6149415E+01	0.7014470E+01	−0.1351834E−02
(2.006, 0, 0)	0.7006000E+01	0.6229685E+01	0.7015476E+01	−0.1352601E−02
(2.008, 0, 0)	0.7008000E+01	0.6385159E+01	0.7017489E+01	−0.1354065E−02
(2.010, 0, 0)	0.7010000E+01	0.6526608E+01	0.7019502E+01	−0.1355435E−02
(2.1, 0, 0)	0.7100000E+01	0.7107873E+01	0.7109472E+01	−0.1334105E−02
(2.5, 0, 0)	0.7500000E+01	0.7501500E+01	0.7503947E+01	−0.5262897E−03
(3.5, 0, 0)	0.8500000E+01	0.8499345E+01	0.8499653E+01	0.4077530E−04
(4.4, 0, 0)	0.9400000E+01	0.9401020E+01	0.9398895E+01	0.1175761E−03
(4.9, 0, 0)	0.9900000E+01	0.9904910E+01	0.9900310E+01	−0.3126717E−04
(5.9, 0, 0)	0.1090000E+02	0.1094649E+02	0.1094710E+02	−0.4321254E−02
(5.99, 0, 0)	0.1099000E+02	−0.1674383E+01	0.1106128E+02	−0.6485760E−02
(5.995, 0, 0)	0.1099500E+02	−0.6643741E+01	0.1106765E+02	−0.6607745E−02

Furthermore, on the inner spherical surface

$$s_1 : x_1^2+x_2^2+x_3^2 = 0.999^2 \quad \text{or} \quad \begin{aligned} x_1 &= 0.999 \sin\phi \cos\theta, \\ x_2 &= 0.999 \sin\phi \sin\theta, \quad 0 \le \theta \le 2\pi, \quad 0 \le \phi \le \pi \\ x_3 &= 0.999 \cos\phi, \end{aligned}$$

500 interior points uniformly spaced according to θ and ϕ, are taken into account. Fig. 2(a) and (b) displays the profiles of the analytical solutions for the potentials u and their derivatives $\partial u/\partial x_1$ on the inner spherical surface S_1, respectively, and Fig. 3(a) and (b) shows the surfaces of the numerical solutions for the potentials u and its derivatives $\partial u/\partial x_1$ at these 500 interior points, respectively. Hence we can see through the comparison of Fig. 2(a, b) and Fig. 3(a, b) that the numerical results match the exact solution very well. Fig. 4 (a) and (b) shows the relative error surfaces of the computational results for the potentials u and their partial derivatives $\partial u/\partial x_1$ at these 500 interior points, where their AREs are $0.83005E-03$ and $0.22921E-02$ at these 500 interior points, respectively. Hence it can be seen that the proposed method is accurate.

Example 2. The second example concerns a problem in a torus centered at origin, as shown in Fig. 5, with the exterior radius and interior radius being $R=4$ and $r=2$, respectively. The parametric equation of the boundary surface is

$$x_1 = (R+r\cos\theta)\cos\phi, \quad x_2 = (R+r\cos\theta)\sin\phi, \quad x_3 = r\sin\theta,$$

$$0 \le \theta \le 2\pi, \quad 0 \le \phi \le 2\pi$$

The prescribed potential distribution along the boundary is

$$u = \tfrac{x^2}{2} + \tfrac{y^2}{2} - z^2 + 5x + 5y + 5z$$

To solve this problem numerically the boundary is discretized by 98 second-order quadrilateral surface elements. Near the boundary of the torus, the interior points increasing close to the real boundary along the direction of axis x_1 are chosen. Table 3 and Table 4 give the numerical solutions for the potentials u and their derivatives $\partial u/\partial x_1$ at these internal points, respectively. Hence it can be seen that when the evaluation points are not too close to the real boundary, the conventional method and the proposed method are both efficient, but the conventional method fails as the evaluation points are closer to the boundary. The two tables also show that as the points approaching the real boundary the relative errors decrease, as would be expected due to the fact that the nearly singular integrals occurred.

Figs. 6 and 7 plot the convergent curves of the potentials and its derivatives at points (2.005,0,0) and (5.995,0,0), respectively. Hence we can observe that the convergence rates of the present method are fast. Furthermore, when the boundary is divided into 180 second-order quadrilateral surface elements, on the inner torus

$$S_2 : \{x_1 = (4+1.99\cos\theta)\cos\phi$$

$$x_2 = (4+1.99\cos\theta)\sin\phi,$$

$$x_3 = 1.99\sin\theta \quad 0 \le \theta \le 2\pi, \quad 0 \le \phi \le 2\pi,$$

540 interior points, uniformly spaced according to θ and ϕ, are taken into account. Fig. 8(a) and (b) displays the profiles of the analytical solutions for the potentials u and their derivatives $\partial u/\partial x_1$ on the inner torus S_2, respectively, and Fig. 9(a) and (b) shows the surfaces of the numerical solutions for the potentials u and their derivatives $\partial u/\partial x_1$ at these 540 interior points, respectively. Hence we can observe from the

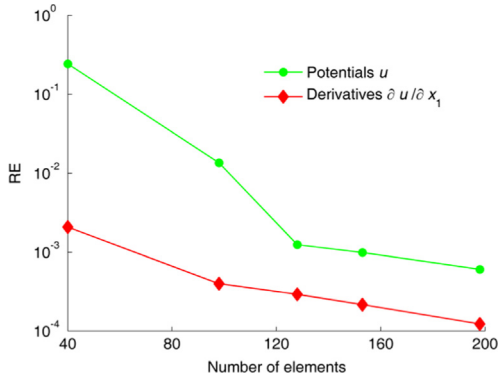

Fig. 6. Convergence curves of u and $\partial u/\partial x_1$ at point $(2.005, 0, 0)$.

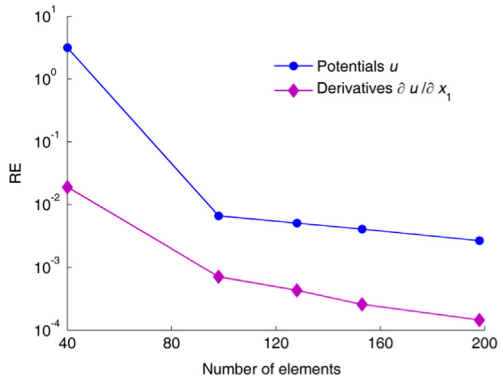

Fig. 7. Convergence curves of u and $\partial u/\partial x_1$ at point $(5.995, 0, 0)$.

comparison of Figs. 8(a, b) and 9(a, b) that the numerical results match the exact solutions very well. Fig. 10(a) and (b) shows the relative error surfaces of the computational results for the potentials u and their partial derivatives $\partial u/\partial x_1$ at these 540 interior points, respectively, where the AREs for the potentials u and their partial derivatives $\partial u/\partial x_1$ at these 540 interior points are $0.2986529E-03$ and $0.1354957E-02$, respectively.

Example 3. As shown in Fig. 11, the last example concerns a thin-body problem in a cylindrical tube Ω. The inner and outer radius are $a=2$ and b, respectively, with b being varying, and the height of the cylinder is $h=6$, i.e.

$$\Omega = \left\{ (x_1, x_2, x_3) \in R^3 : a < \sqrt{x_1^2 + x_2^2} < b, \quad -3 < x_3 < 3 \right\}.$$

A mixed boundary condition is given on the boundary Γ. On the top and bottom face $\{a \le \sqrt{x_1^2+x_2^2} \le b, \quad x_3 = \pm 3\}$ and the outer surface $\{\sqrt{x_1^2+x_2^2} = b, \quad -3 < x_3 < 3\}$, the Dirichlet boundary condition is prescribed $u = \overline{u}$, while on the remaining components of Γ, it is the Neumann boundary condition $q = \overline{q} = n\nabla u$, with

$$\overline{u} = x_1^3 + 2x_2^3 + 3x_3^3 - 3x_1x_3^2 - 6x_2x_1^2 - 9x_3x_2^2$$

$$\nabla u = (3x_1^2 - 3x_3^2 - 12x_1x_2, \quad -6x_1^2 + 6x_2^2 - 18x_2x_3, \quad -9x_2^2 + 9x_3^2 - 6x_1x_3)$$

To solve the problem numerically, both the outside face and the inside face are divided into 40 second-order quadrilateral paraboloidal surface elements, and the 8 second-order quadrilateral flat surface elements are employed on both the top face and the bottom face. In this example, $\beta = (b-a)/a$ is defined as the thickness-to-length ratio. As a is fixed as 2, the ratio reduces as b decreases.

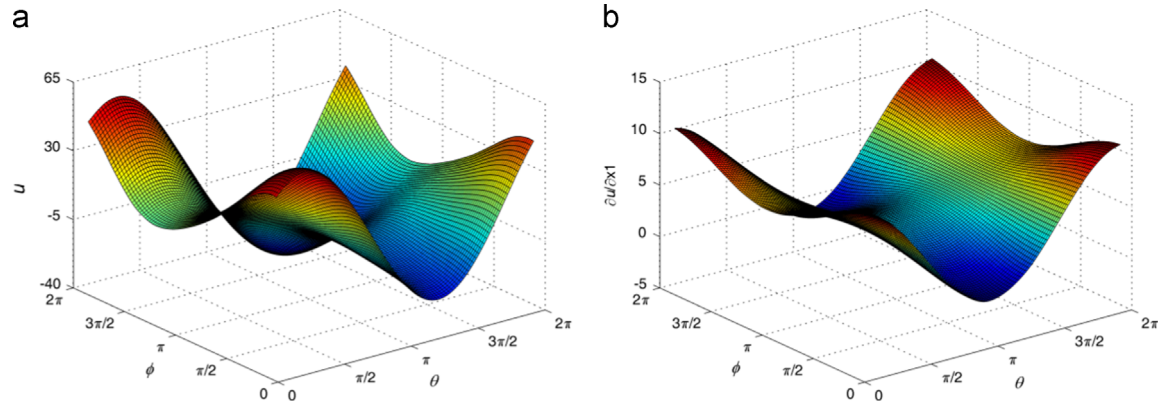

Fig. 8. Profiles of analytical solutions: for the potentials (a) and their derivatives (b).

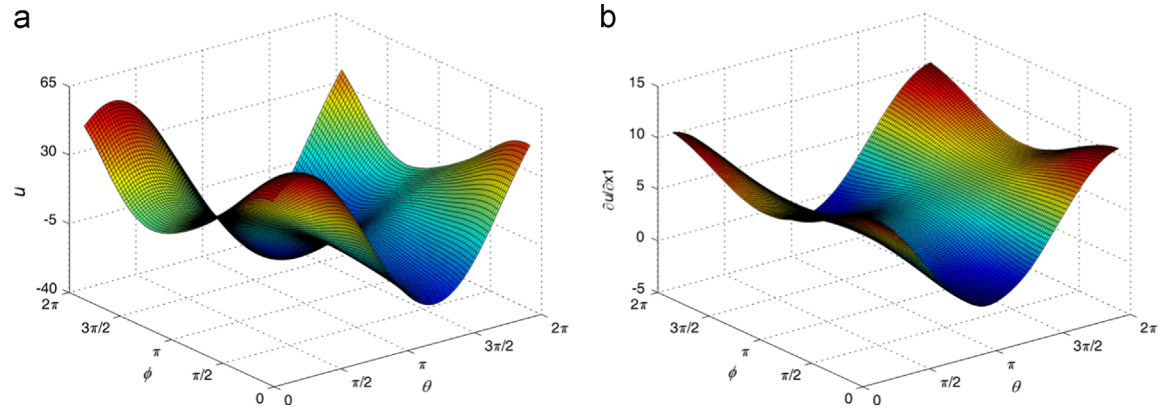

Fig. 9. Profiles of numerical solutions for the potentials (a) and its derivatives (b).

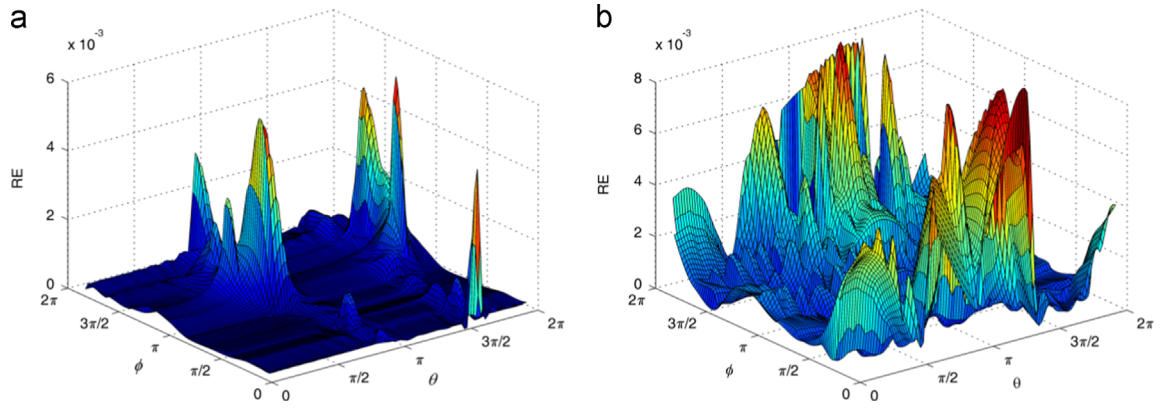

Fig. 10. Surfaces of REs for the potentials (a) and their derivatives (b).

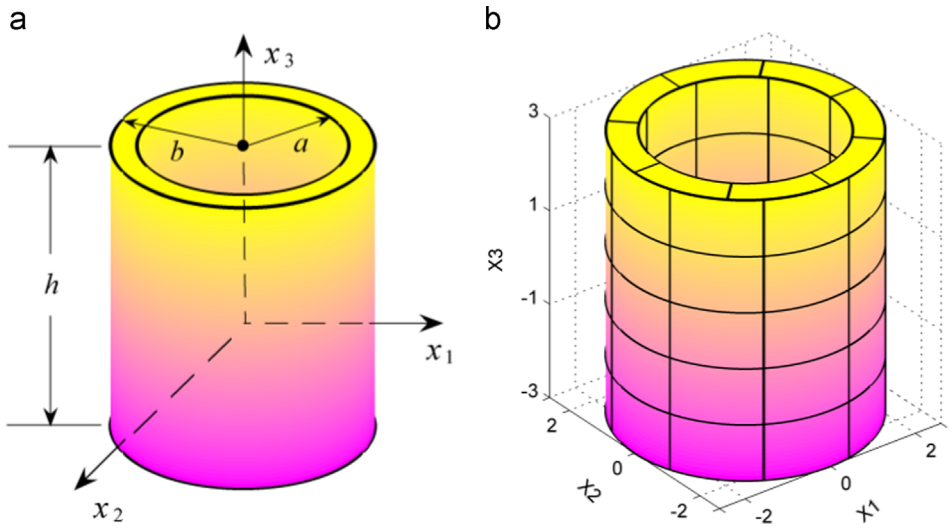

Fig. 11. (a) Thin-body cylindrical tube and (b) meshes on its boundary.

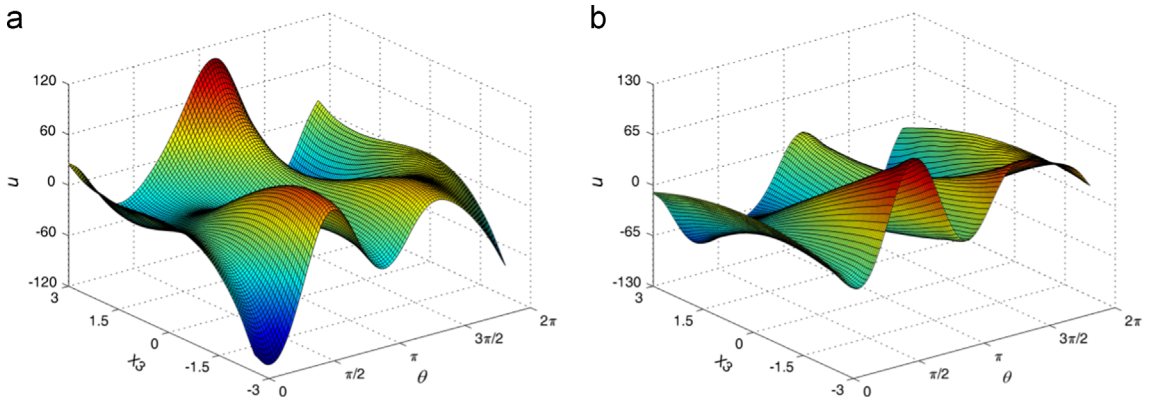

Fig. 12. Profiles of analytical solutions: (a) potentials on the inner surface and (b) fluxes on the outside surface.

When $\beta = 5.0E-06$, Fig. 12(a) and (b) displays the profiles of the analytical solutions for the potentials u on the inner surface and their derivatives $\partial u/\partial \mathbf{n}$ on the outside surface, respectively, and Fig. 13 (a) and (b) shows the surfaces of the numerical solutions for the potentials u on the inner surface and its derivatives $\partial u/\partial n$ on the outside surface, respectively. Hence we can see through the comparison of Fig. 12(a, b) and Fig. 13(a, b) that the numerical results match the exact solution very well. Fig. 14(a) and (b) shows the relative error surfaces of the computational results for the potentials u on the inner surface and their partial derivatives $\partial u/\partial n$ on the outside surface. Hence it can be seen that the proposed method is accurate.

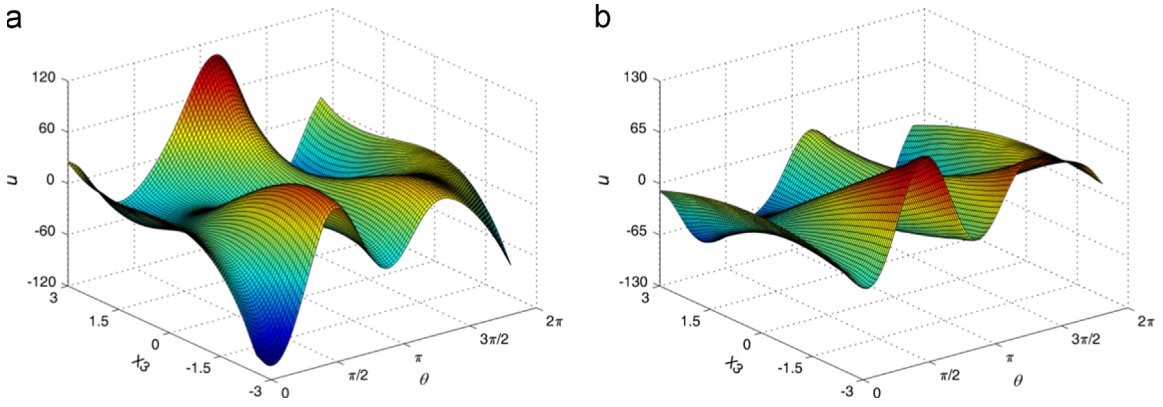

Fig. 13. Surfaces of numerical solutions: (a) potentials on the inner surface and (b) fluxes on the outside surface.

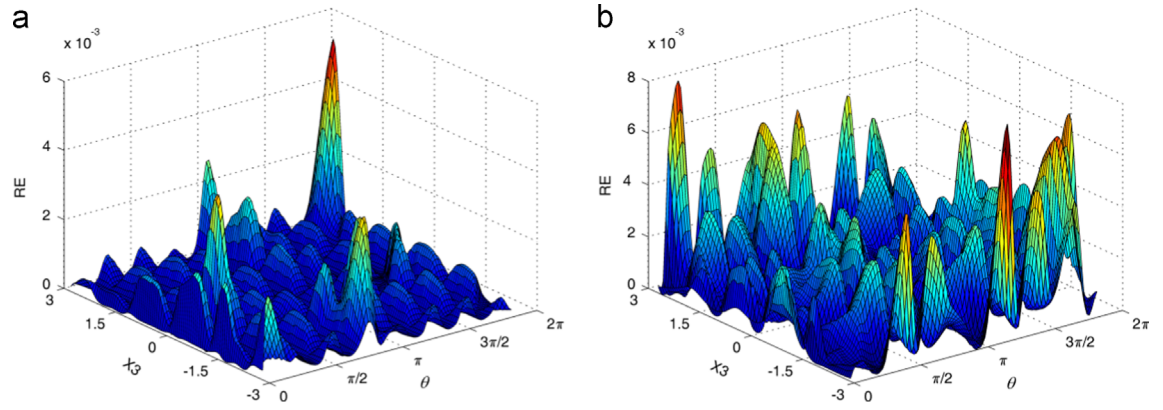

Fig. 14. RE surfaces of numerical results: (a) potentials on the inner surface and (b) fluxes on the outside surface.

6. Conclusions

This study presents an improved scheme in order to numerically calculate 2D nearly singular integrals arising in 3D BEM. The scheme is an extension of the sinh transformation, which is used to evaluate the 1D or 2D nearly singular integrals on simple geometry elements, such as usual linear or planar elements, to 3D BEM using the eight-node second-order quadrilateral surface element. Three numerical examples with exact benchmark solutions are presented to test the proposed scheme, yielding very promising results. The results verify the feasibility and the effectiveness of the proposed scheme.

Acknowledgments

The support from the Opening Fund of the State Key Laboratory of Structural Analysis for Industrial Equipment (GZ1017) and the National Natural Science Foundation of Shangdong Province of China (ZR2010AZ003) are gratefully acknowledged.

References

[1] Luo JF, Liu YJ, Berger EJ. Analysis of two-dimensional thin structures (from micro- to nano-scales) using the boundary element method. Comput Mech 1998;22(5):404–12.
[2] Gao XW, Yang K, Wang J. An adaptive element subdivision technique for evaluation of various 2D singular boundary integrals. Eng Anal Bound Elem 2008;32:692–6.
[3] Niu ZR, Cheng CZ, Zhou HL, Hu ZJ. Analytic formulations for calculating nearly singular integrals in two-dimensional BEM. Eng Anal Bound Elem 2007;31(12):949–64.
[4] Mukerjee S, Chati MK, Shi XL. Evaluation of nearly singular integrals in boundary element contour and node methods for three-dimensional linear elasticity. Int J Solids Struct 2000;37:7633–54.
[5] Liu YJ. Analysis of shell-like structures by the boundary element method based on 3-D elasticity: formulation and verification. Int J Numer Methods Eng 1998;41:541–58.
[6] Zhang YM, Gu Y, Chen JT. Stress analysis for multilayered coating systems using semi-analytical BEM with geometric non-linearities. Comput Mech 2011;47(5):493–504.
[7] Shiah YC, Shih YS. Regularization of nearly singular integrals in the boundary element analysis for interior an isotropic thermal field near the boundary. Eng Anal Bound Elem 2007;30(2):219–30.
[8] Cerrolaza M, Alarcon E. A bi-cubic transformation for the numerical evaluation of the Cauchy principal value integrals in boundary methods. Int J Numer Meth Eng 1989;28(5):987–99.
[9] Letizia Scuderi. A new smoothing strategy for computing nearly singular integrals in 3D Galerkin BEM. J Comput Appl Math 2009;225:406–27.
[10] Ye WJ. A new transformation technique for evaluating nearly singular integrals. Comput Mech 2008;42:457–66.
[11] Sladek V, Sladek J, Tanaka M. Optimal transformations of the integration variables in computation of singular integrals in BEM. Int J Numer Methods Eng 2000;47(7):1263–83.
[12] Johnston PR. Application of Sigmoidal transformations to weakly singular and near singular boundary element integrals. Int J Numer Methods Eng 1999;45(10):1333–48.
[13] Johnston BM, Johnston PR, Elliott D. A new method for the numerical evaluation of nearly singular integrals on triangular elements in the 3D boundary element method. J Comput Appl Math 2013;245:148–61.
[14] Johnston PR, Elliott D. A sinh transformation for evaluating nearly singular boundary element integrals. Int J Numer Methods Eng 2005;62(4):564–78.
[15] Johnston BM, Johnston PR, Elliott D. A sinh transformation for evaluating two-dimensional nearly singular boundary element integrals. Int J Numer Methods Eng 2007;69(7):1460–79.
[16] Elliott D, Johnston PR. The iterated sinh transformation. Int J Numer Methods Eng 2008;75(1):43–57.
[17] Johnston PR, Johnston BM, Elliott D. Using the iterated sinh transformation to evaluate two dimensional nearly singular boundary element integrals. Eng Anal Bound Elem 2013;37:708–18.
[18] Lv JH, Miao Y, Gong WH, Zhu HP. The sinh transformation for curved elements using the general distance function. Comput Model Eng Sci 2013;93(2):113–31.

[19] Lv JH, Miao Y, Zhu HP. The distance sinh transformation for the numerical evaluation of nearly singular integrals over curved surface elements. Comput Mech 2014;53(2):359–67.
[20] Huang Q, Cruse TA. Some notes on singular integral techniques in boundary element analysis. Int J Numer Methods Eng 1993;36(15):2643–59.
[21] Ma H, Kamiya N. Distance transformation for the numerical evaluation of near singular boundary integrals with various kernels in boundary element method. Eng Anal Bound Elem 2002;26(4):329–39.
[22] Ma H, Kamiya N. A general algorithm for the numerical evaluation of nearly singular boundary integrals of various orders for two-and three-dimensional elasticity. Comput Mech 2002;29:277–88.
[23] Qin XY, Zhang JM, Xie GZ, Zhou FL, Li GY. A general algorithm for the numerical evaluation of nearly singular integrals on 3D boundary element. J Comput Appl Math 2011;235:4174–86.
[24] Miao Y, Li W, Lv JH, Zhu HP. Distance transformation for the numerical evaluation of nearly singular integrals on triangular elements. Eng Anal Bound Elem 2013;37(10):1311–7.
[25] Zhang YM, Sun CL. A general algorithm for the numerical evaluation of nearly singular boundary integrals in the equivalent non-singular BIEs with indirect unknowns. J Chin Inst Eng 2008;31(3):437–47.
[26] Zhang YM, Gu Y, Chen JT. Boundary layer effect in BEM with high order geometry elements using transformation. Comput Model Eng Sci 2009;45 (3):227–47.
[27] Zhang YM, Gu Y, Chen JT. Internal stress analysis for single and multilayered coating systems using the boundary element method. Eng Anal Bound Elem 2010;35(4):708–17.
[28] Zhang YM, Qu WZ, Chen JT. BEM analysis of thin structures for thermoelastic problems. Eng Anal Bound Elem 2013;37:441–52.
[29] Xie GZ, Zhou FL, Zhang JM, Zheng XS, Huang C. New variable transformations for evaluating nearly singular integrals in 3D boundary element method. Eng Anal Bound Elem 2013;37:1169–78.
[30] Zhang YM, Li XC, Sladek V, Sladek J. A general algorithm for calculating nearly singular integrals over high-order elements in 3D BEM. Chin J Theor Appl Mech 2013;45(6):908–18.